5016 *Inorg. Chem.* **2010**, *49*, 5016–5024
DOI: 10.1021/ic1001732

Inorganic Chemistry
Article

Synthesis and Structural Characterization of Cationic 5-Hydroxy-1,3-diketonate Stabilized Dinuclear Complexes and Tetranuclear Lanthanoid Clusters

Philip C. Andrews, William J. Gee, Peter C. Junk,* and Jonathan G. MacLellan

School of Chemistry, Monash University, Victoria, Clayton 3800, Australia

Received January 28, 2010

5-Hydroxy-1,3-diketonate ligands have been found to stabilize dimeric complexes and tetrameric lanthanoid clusters dependent on the degree of steric bulk provided by the presence or absence of a methoxy group. Treatment of (*R*/*S*,*Z*)-1′-hydroxy-3-(hydroxy(phenyl)methylene)bi(cyclopentan)-2-one (**Hhpb**) and the *p*-methoxyphenyl derivative (**Hhmb**) with $[LnCl_2(H_2O)_6]Cl$ yields clusters of composition $[Ln_4(Cl)_2(O)(\mathbf{hpb})_6]Cl_2$ (Ln = Nd (**1**), Ho (**2**), Tb (**3**), and Er (**4**)) and $[Ln_2(\mathbf{hmb})_5]Cl$ (Ln = La (**5**), Nd (**6**), Tb (**7**), Dy (**8**), and Er (**9**)). Single crystal X-ray analysis of the tetranuclear cluster has revealed the lanthanoid core to be in a tetrahedral arrangement around a central μ_4-oxygen, bridged by symmetrical chlorides and shrouded in six bridging **hpb** ligands. The dimeric complexes are stabilized by three bridging and two terminal **hmb** ligands. In each instance, double or single cationic charges respectively are balanced by chloride anions.

Introduction

The chemistry of lanthanoid diketonate clusters has expanded in recent years to include a diverse range of nuclearities and structural motifs.[1] The initial well-characterized example of this family, an octanuclear erbium cluster, was first reported in 1972.[2] Since this time, the chemistry of diketonate clusters has continually expanded and currently includes dinuclear,[3] trinuclear,[4] tetranuclear,[5−10] pentanuclear,[7,10−13] hexanuclear,[14] octanuclear,[11] nonanuclear,[11,15−19] and dodecanuclear[20] clusters. Of these cluster motifs, the majority are neutral species, the exceptions being (i) nonanuclear compounds, which may be neutral,[11] or either positively[17−19] or negatively charged,[15,16] and (ii) a serendipitous cationic trinuclear holmium complex.[4]

The intrinsic luminescent,[11,21−27] magnetic,[12,28,29] and Lewis acidic properties of the lanthanoid metals means that there is great potential for such clusters to find application in chemical sensing, biological chemistry, medicine, and catalysis.[7] While simple mononuclear lanthanoid compounds may already be considered to be ubiquitous in these areas, exploring the unique chemistry of the clusters and progressing from mere possibility to actual application has

*To whom correspondence should be addressed. E-mail: peter.junk@sci.monash.edu.au.

(1) Zheng, Z. *Handbook on the Physics and Chemistry of Rare Earths Elements*; Gschneidner, K. A., Jr.; Bünzli, J.-C. G.; Pecharsky, V. K.; Elsevier: Amsterdam, 2010; Vol. *40*, p 109.
(2) Boeyens, J. C. A.; De Villiers, J. P. R. *J. Cryst. Mol. Struct.* **1972**, *2*, 197.
(3) Brück, S.; Hilder, M.; Junk, P. C.; Kynast, U. H. *Inorg. Chem. Commun.* **2000**, *3*, 666.
(4) Andrews, P. C.; Deacon, G. B.; Frank, R.; Fraser, B. H.; Junk, P. C.; MacLellan, J. G.; Massi, M.; Moubaraki, B.; Murray, K. S.; Silberstein, M. *Eur. J. Inorg. Chem.* **2009**, *6*, 744.
(5) Baskar, V.; Roesky, P. W. *Z. Anorg. Allg. Chem.* **2005**, *631*, 2782.
(6) Baskar, V.; Roesky, P. W. *Dalton Trans.* **2006**, 676.
(7) Roesky, P. W.; Canseco-Melchor, G.; Zulys, A. *Chem. Commun.* **2004**, 738.
(8) Bürgstein, M. R.; Gamer, M. T.; Roesky, P. W. *J. Am. Chem. Soc.* **2004**, *126*, 5213.
(9) Bürgstein, M. R.; Roesky, P. W. *Angew. Chem., Int. Ed.* **2000**, *39*, 594.
(10) Andrews, P. C.; Beck, T.; Fraser, B. H.; Junk, P. C.; Massi, M.; Moubaraki, B.; Murray, K. S.; Silberstein, M. *Polyhedron* **2009**, *28*, 2123.
(11) Petit, S.; Baril-Robert, F.; Pilet, G.; Reber, C.; Luneau, D. *Dalton Trans.* **2009**, 6809.
(12) Gamer, T. M.; Lan, Y.; Roesky, P. W.; Powell, A. K.; Clerac, R. *Inorg. Chem.* **2008**, *47*, 6581.
(13) Datta, S.; Baskar, V.; Li, H.; Roesky, P. W. *Eur. J. Inorg. Chem.* **2007**, 4216.
(14) Jami, A. K.; Kishore, P. V. V. N.; Baskar, V. *Polyhedron* **2009**, *28*, 2284.
(15) Hubert-Pfalzgraf, L. G.; Meile-Pajot, N.; Papiernik, R.; Vaissermann, J. *J. Chem. Soc., Dalton Trans.* **1999**, 4127.
(16) Xu, G.; Wang, Z. M.; He, Z.; Lu, Z.; Liao, C. S.; Yan., C. H. *Inorg. Chem.* **2002**, *41*, 6802.
(17) Addamo, M.; Bombieri, G.; Foresti, E.; Grillone, M. D.; Volpe, M. *Inorg. Chem.* **2004**, *43*, 1603.
(18) Bombieri, G.; Clemente, D. A.; Foresti, E.; Grillone, M. D.; Volpe, M. *J. Alloys Compd.* **2004**, *374*, 382.
(19) Volpe, M.; Bobmieri, G.; Clemente, D. A.; Foresti, E.; Grillone., M. D. *J. Alloys Compd.* **2006**, *406*, 1046.
(20) Andrews, P. C.; Beck, T.; Forsyth, C. M.; Fraser, B. H.; Junk, P. C.; Massi, M.; Roesky, P. W. *Dalton Trans.* **2007**, 5651.
(21) Zhang, L. Z.; Gu, W.; Li, B.; Liu, X.; Liao, D. Z. *Inorg. Chem.* **2007**, *46*, 622.
(22) Bünzli, J. C. G. *Acc. Chem. Res.* **2006**, *39*, 53.
(23) Xiong, R. G.; Zuo, J. L.; Yu, Z.; You, X. Z.; Chen, W. *Inorg. Chem. Commun.* **1999**, 490.
(24) Sabbatini, N.; Guardigli, M. *Coord. Chem. Rev.* **1993**, *123*, 201.
(25) de Su, G. F.; Malta, O. L.; Donega, C. D.; Simas, A. M.; Longo, R. L.; Santa-Cruz, P. A.; da Silva, E. F. *Coord. Chem. Rev.* **2000**, *196*, 165.
(26) Kido, J; Okamoto, Y. *Chem. Rev.* **2002**, *102*, 2357.
(27) Bunzli, J. C. G.; Piguet, C. *Chem. Soc. Rev.* **2005**, *34*, 1048.
(28) Benelli, C.; Gutteschi, D. *Chem. Rev.* **2002**, *102*, 2369.
(29) Sessoli, R.; Powell, A. K. *Coord. Chem. Rev.* **2009**, *253*, 2328.

Published on Web 04/29/2010

Scheme 1.[a]

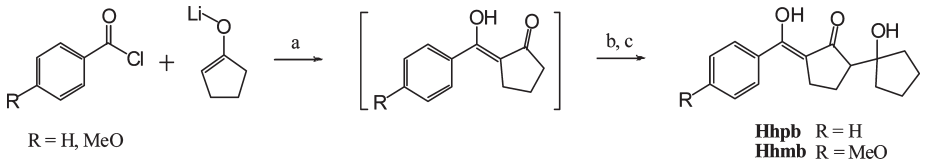

[a] Reagents and conditions: (a) THF, −78 °C, 5 min; (b) 2 equiv LiHMDS, 5 min; (c) 1 equiv cyclopentanone, −78 °C→RT, 2 h.

been relatively slow. This is because the large majority of lanthanoid oxo/hydroxo clusters have only been prepared and isolated serendipitously, with little design or control. However, a substantial number and variety of neutral clusters now exist that makes it possible to gain some insight and understanding into their chemistry. In contrast, there remains a paucity of information on the synthesis, isolation, and properties of analogous charged species.

An analysis of the structural types observed for the various clusters suggests a trend inversely linking cluster size to the degree of hindrance offered by the ligand. As such, the dominance of neutral clusters in the literature can be attributed to a bias in using compact ligands with open, easily accessible chelation regions. Such ligands, while actively aiding cluster growth by facilitating the conversion of coordinated water molecules to the oxo- and hydroxo- components of the metal cage core, promote a final neutral charge on the metal oxo/hydroxo core through the lack of steric hindrance offered by the ligands to incoming water molecules.

It follows that stable cationic cluster species of varying nuclearity should be accessible through opposing this trend, that is, designing and using ligands with sufficient steric bulk and with multiple coordination sites that allow cluster growth but would displace coordinated water from the cluster core. The lack of coordination of water to the metal ions and sufficient shielding of the ligands from secondary deprotonation would ensure that the cationic charge of the cluster core could not be completely offset.

In this paper, we now report the syntheses of two new series of cationic lanthanoid diketonate clusters, including the synthetic pathway to a chloride-bridged tetrahedral motif using an air- and moisture-stable methodology. The clusters are stabilized by two new ligands: (*R*/*S*,*Z*)-1′-hydroxy-3-(hydroxy(phenyl)methylene)-bi(cyclopentan)-2-one (**Hhpb**) and the corresponding *p*-methoxyphenyl derivative (**Hhmb**), which give clusters of composition $[Ln_4(Cl)_2(O)(\mathbf{hpb})_6]Cl_2$ (Ln = Nd (**1**), Ho (**2**), Tb (**3**), and Er (**4**)) and $[Ln_2(\mathbf{hmb})_5]Cl$ (Ln = La (**5**), Nd (**6**), Tb (**7**), Dy (**8**), and Er (**9**)). The cationic nature of the clusters is a result of ligand design, whereby coordinating hydroxy groups of the tridentate ligands are masked by bulky cyclopentane rings which prevent basic attack, ensuring a monoanionic charge on each ligand.

The tricyclic 5-hydroxy-1,3-diketones, **Hhpb** and **Hhmb**, were obtained in moderate yields by a rapid one-pot synthetic procedure and have been fully characterized using standard spectroscopic techniques including **Hhpb** by single crystal X-ray diffraction. Cluster formation was achieved by a variation of "ligand controlled hydrolysis",[30] whereby displacement of already present coordinated water molecules with shielding ligands culminates in a finite number of resultant hydroxo and oxo species capable of generating the core structure.

(30) Wang, R.; Liu, H.; Carducci, M. D.; Jin, T.; Zheng, C.; Zheng, Z. *Inorg. Chem.* **2001**, *40*, 2743.

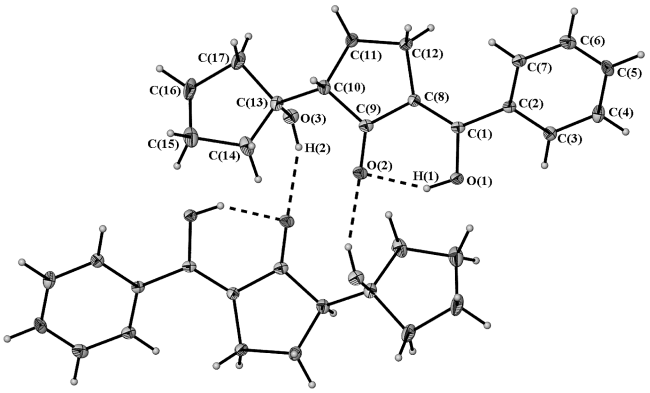

Figure 1. Molecular structure of **Hhpb** showing hydrogen bonding interactions between two molecules. Thermal ellipsoids are shown at 50% probability.

Tetranuclear lanthanoid clusters **1**−**4** were characterized by Raman and infrared spectroscopy, elemental and thermogravimetric analysis, mass spectrometry, and in the case of **1**, single crystal X-ray crystallography. Dinuclear lanthanoid clusters **5**−**9** were characterized by infrared spectroscopy, elemental and thermogravimetric analysis, mass spectrometry, and single crystal X-ray crystallography for **5** and **7**.

Results and Discussion

The 5-hydroxy-1,3-diketones used in this study were synthesized by a rapid, one-pot reaction proceeding via formation of a 2-benzoylcyclopentanone intermediate. The intermediate was treated with lithium hexamethyldisilazide (LiHMDS) and cyclopentanone (Scheme 1), yielding the desired ligands after purification by column chromatography. Moderate yields for both ligands were obtained, ranging from 56% for **Hhpb** to 63% for **Hhmb**.

Solution state ^{1}H NMR analysis of **Hhpb** and **Hhmb** determined that each primarily exists as the enol tautomer, as identified by resonances corresponding to the enolic proton at 14.49 and 14.64 ppm, respectively. The minor keto tautomer was detected as a triplet at 4.25 ppm for **Hhpb** and a doublet of doublets at 4.21 ppm for **Hhmb** corresponding to a proton at the α position. The ratio of keto and enol tautomerism was determined to be 1:5 and 1:2.5, respectively. A solid state structure of **Hhpb** was obtained by single crystal X-ray diffraction (Figure 1). The enol form was identified via assignment of residual electron density to the enol proton H(1) and the hydroxy proton H(2). Furthermore, the planar geometry (sum of bond angles is 359.99°) around C(2) confirms the presence of the enol tautomer. In the extended crystal structure, two antiparallel molecules are offset such that they link through hydrogen bonding from the hydroxy group of one molecule to the ketone oxygen of its neighbor.

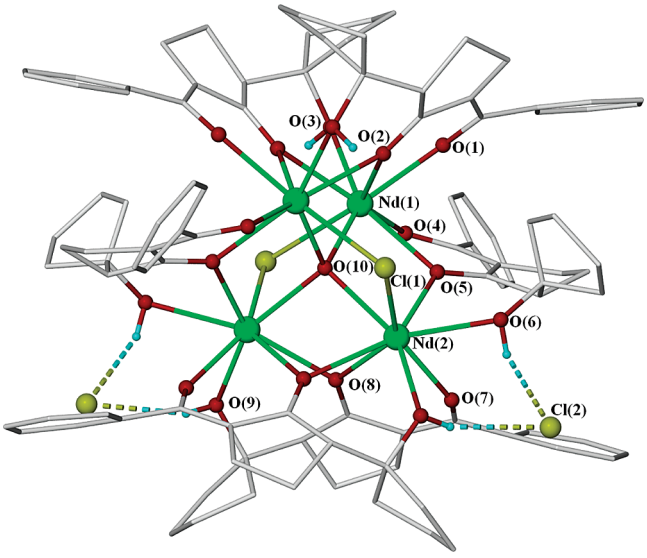

Figure 2. Molecular structure of **1**. Lattice solvent and H atoms (excluding hydroxy) have been omitted for clarity.

Cationic lanthanoid clusters were synthesized by the reaction of two equivalents of the respective ligand with one equivalent of $[LnCl_2(H_2O)_6]Cl$ in the presence of methanolic triethylamine. Subsequent removal of the methanol under reduced pressure followed by dissolution in toluene resulted in precipitation of triethylamine hydrochloride, enabling isolation of solvated pure compounds after filtration. Depending on the ligand employed, tetrameric clusters of composition $[Ln_4(Cl)_2(O)(\mathbf{hpb})_6]Cl_2$ (Ln = Nd (**1**), Ho (**2**), Tb (**3**), and Er (**4**)) or dimeric complexes of $[Ln_2(\mathbf{hmb})_5]Cl$ (Ln = La (**5**), Nd (**6**), Tb (**7**), Dy (**8**), and Er (**9**)) were obtained.

Crystals of tetranuclear clusters (**1**−**4**) were difficult to obtain; however, slow diffusion of diethyl ether into a solution containing **1** in wet dimethylformamide yielded single crystals after four weeks (Figure 2). The solid state structure was then determined by single crystal X-ray analysis.

The structure of **1** is shown in Figure 2, and a list of selected bond lengths and angles is given in Table 1. The tetranuclear cluster that resides on a 2-fold axis consists of a central μ_4-oxo core with the Nd atoms bonded in a distorted tetrahedral arrangement. Nd−O(oxide) distances are identical at 2.362(4) Å and 2.366(4) Å; the Nd−O−Nd angles average 107.4° and range from 100.1(3)° to 118.01(3)°. Within the cluster core, two μ_2-chloride anions bridge opposing pairs of Nd atoms with Nd−Cl bonds of 2.850(2) Å and 2.844(2) Å and Nd−Cl−Nd angles of 90.77(7)°. Nd atoms are also μ_2-bridged by the central O atom of each of the six ligands surrounding the core. Each Nd is coordinated by three ligands. Nd(1) is bound in a η^2(O,O′) fashion to two ligands through the diketyl moiety, and the third ligand binds η^2(O′,OH) through the central oxygen atom and the hydroxy oxygen atom. Nd(2) is bound by two ligands in a η^2(O′,OH) fashion and just one via η^2(O,O′) bonding. This gives each ligand an overall binding mode of μ_2-η^2(O,O′)η^2(O′,OH). Combined with the interactions of the chloride and central oxide, these six Nd−O bonds result in an overall coordination number of eight around the metal centers. The outer diketyl oxygen atom has the shortest Nd−O bond lengths, averaging 2.37 Å, whereas the central, bridging diketyl oxygen has Nd−O bond lengths averaging 2.50 Å. The terminal OH average distance is 2.47 Å. The two "bite angles" provided by these ligands vary slightly (average 69.5° and 73.1°) with the larger angle belonging to the "bite" contained by the slightly elongated Nd−O(H) bonds. Due to the steric bulk and coordinative saturation provided by the ligand, only six shroud the core. This leaves a dicationic charge which is balanced by two chloride anions in the outer coodination sphere of the cluster. These chloride ions are held to the cluster by hydrogen bonding to two hydroxy groups with donor−acceptor distances of 3.007(7) and 3.018(7) Å. The remaining two hydroxy groups per cluster H-bond to DMF solvent molecules (donor−acceptor distance 2.645(10) Å). A number of solvent accessible voids exist between the clusters, and these can tentatively be assigned to molecules of diethyl ether. However, large amounts of disorder, thermal motion, and the comparatively miniscule amount of electron density mean that they cannot be satisfactorily modeled. One example of this motif type has been reported previously containing yttrium, albeit as a neutral species isolated in low yield.[31]

Table 1. Selected Bond Lengths and Angles for **1**[a]

Bond Lengths, Å			
Nd(1)−O(1)*	2.353(6)	Nd(2)−O(5)	2.432(6)
Nd(1)−O(2)	2.534(6)	Nd(2)−O(6)	2.508(6)
Nd(1)−O(2)*	2.562(6)	Nd(2)−O(7)*	2.349(6)
Nd(1)−O(3)	2.453(6)	Nd(2)−O(8)	2.467(6)
Nd(1)−O(4)*	2.396(6)	Nd(2)−O(8)*	2.544(6)
Nd(1)−O(5)*	2.443(6)	Nd(2)−O(9)	2.461(6)
Nd(1)−O(10)	2.362(4)	Nd(2)−O(10)	2.366(4)
Nd(1)−Cl(1)	2.850(2)	Nd(2)−Cl(1)	2.844(2)
Bond Angles, deg			
O(1)−Nd(1)*−O(2)	67.9(2)	O(5)−Nd(2)−O(6)	72.9(2)
O(2)−Nd(1)−O(3)	72.6(2)	O(7)−Nd(2)*−O(8)	68.9(2)
O(4)−Nd(1)*−O(5)	71.6(2)	O(8)−Nd(2)−O(9)	73.7(2)

[a] Symmetry operator (*): $-x, y, -z + 1/2$.

Exhaustive attempts at growing single crystals suitable for X-ray crystallography for clusters **2**−**4** were unsuccessful; hence, identification of these species was performed using standard spectroscopic techniques. Recently, a literature precedent has emerged utilizing Raman spectroscopy to identify the distinctive "fingerprints" inherent in a lanthanoid cluster core.[11] While the spectra themselves are complex and individual resonances remain undetermined, the motif contains unique Ln−Cl−Ln and Ln−O−Ln bands in an arrangement active to Raman spectroscopy for analysis and comparison. Unfortunately, the neodymium cluster was found to fluoresce at a wavelength of 782 nm, coinciding with the emission wavelength of the Renishaw diode laser. Similar luminescent emissions have been observed from complexes incorporating neodymium at approximately this wavelength.[32] As a result, analysis using a second laser source emitting at 514 nm was undertaken, which elucidated weakened intensities for bands in the region of 200 to 750 cm^{-1}. The Raman spectra of **2**−**4** are compared with that of the known cluster **1** (Figure 3). Consistent overlap of bands is observed between the four species over the region of 800 to 2000 cm^{-1}. At lower wavenumbers, the peak intensities for **1** and **3** are too weak for a definitive comparison, preventing confirmation of the cluster motif by this technique alone.

(31) Coles, M. P.; Hitchcock, P. B. *Inorg. Chim. Acta* **2004**, *357*, 4330.
(32) Gonçalves, M. C.; Silva, N. J. O.; de Zea Bermudez, V.; Sá Ferreira, R. A.; Carlos, L. D.; Dahmouche, K.; Santilli, C. V.; Ostrovskii, D.; Correia Vilela, I. C.; Craievich, A. F. *J. Phys. Chem. B* **2005**, *109*, 20093.

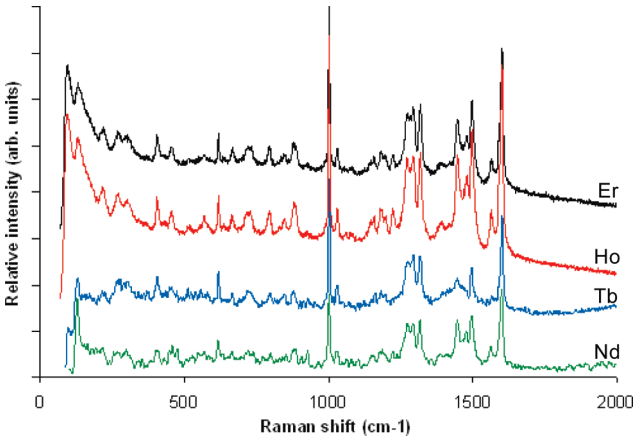

Figure 3. Raman spectra of Nd (**1**), Ho (**2**), Tb (**3**), and Er (**4**).

A comparison of the infrared spectra obtained for complexes **1**−**4** illustrates identical features from 4000 to 500 cm^{-1}. Twin resonances at 1592 and 1565 cm^{-1}, corresponding to the υ(C═C) and υ(C═O) vibrations, are prominent and shifted to lower wavenumbers compared with the free ligand at 1639 and 1607 cm^{-1}. Broadened bands at 1447 and 1370 cm^{-1} correspond to aromatic υ(C═C) stretch absorptions, and a medium intensity band at 1264 cm^{-1} was attributed to a ketone-bending mode.[33,34]

Elemental analyses performed on a vacuum-dried crystalline sample of **1** and bulk samples for compounds **2**−**4** gave results consistent with solvates. As recrystallization proved impossible for compounds **2**−**4**, a low hydrogen percentage is indicative of small amounts of lanthanoid chloride containing intermediates present in these samples. Thermogravimetric analysis was used to compare the thermal degradation pathway for compounds **1**−**4**. Weight loss percentages of between 4.22% and 8.63% were observed over a temperature range of 50 to 200 °C. We postulate that these losses represent liberation of solvent molecules from the crystal lattice, combined with four equivalents of HCl displaced by secondary deprotonation of the ligands. A comparison of the weight loss profiles for complexes **1**−**4** from 200 to 650 °C shows a near identical thermal degradation pathway. In all four cases, the onset of the first incremental loss corresponding to 15% by weight occurs within the range of 272.4−282.3 °C. Secondary losses of 15% (onset temp: 275 °C) and 10% (onset temp: 517 °C) were seen to occur in a similar concurrent manner. These losses are attributed to degradation of the ligand to give simple volatile components. It is likely that lanthanoid oxide species and charred remnants of the ligand make up the remaining 50% by weight present after heating has concluded.

An analysis of **1**−**4** by electrospray mass spectrometry (ESI-MS) gave cationic fragments formed by dissociation of the cluster (Table 2). Dominant species are listed with the proposed molecular formula. In each case, only the most prominent isotope is reported.

Analyses of these fragments allow us to postulate the fragmentation pathway (Scheme 2) for each cluster species.

(33) Nakamoto, K. *Infrared and Raman Spectra of Inorganic and Coordination Compounds*, 4th ed.; Wiley-Interscience Publication: New York, 1986; p 259.
(34) Junge, H.; Musso, H. *Spectrochim. Acta, Part A* **1968**, *A24*, 1219.

Table 2. Assignment of Charged Species Observed for Clusters **1**−**4** by ESI(+)-MS

cationic species	*m*/*z* (calculated)	*m*/*z* (found)
$[Nd(\mathbf{hpb})(OH)(MeO)]Na^+ \cdot MeOH$	516.1	516.2
$[Nd(\mathbf{hpb})(OH)(MeO)]Na^+ \cdot 3MeOH$	548.1	548.2
$[Nd(\mathbf{hpb})(OH)(MeO)]Na^+ \cdot 2MeOH$	580.2	580.2
$[Nd(\mathbf{hpb})_2(MeO)]Na^+$	738.2	738.1
$[Nd_2(O)(\mathbf{hpb})_2(MeO)]^+$	875.1	876.3
$[Nd_2(O)(\mathbf{hpb})_3]^+$	1115.2	1114.5
$[Nd_4(Cl)_2(O)(\mathbf{hpb})_6]^{2+}$	1143.7	1142.6
$[Nd_4(OH)_2(O)(\mathbf{hpb})_6]^{2+} \cdot 2MeOH$	1157.7	1157.1
$[Nd_4(OH)_2(O)(\mathbf{hpb})_6]^{2+} \cdot 6MeOH$	1222.3	1223.2
$[Ho(\mathbf{hpb})(OH)(MeO)]Na^+ \cdot MeOH$	539.1	539.2
$[Ho(\mathbf{hpb})(OH)(MeO)]Na^+ \cdot 2MeOH$	571.1	571.3
$[Ho(\mathbf{hpb})(OH)(MeO)]Na^+ \cdot 3MeOH$	603.2	603.2
$[Ho_4(OH)_2(O)(\mathbf{hpb})_6]^{2+} \cdot 2MeOH$	1200.8	1201.2
$[Ho_4(OH)_2(O)(\mathbf{hpb})_6]^{2+} \cdot 6MeOH$	1264.8	1265.1
$[Tb(\mathbf{hpb})(OH)(MeO)]Na^+ \cdot MeOH$	533.1	532.9
$[Tb(\mathbf{hpb})(OH)(MeO)]Na^+ \cdot 2MeOH$	565.1	564.9
$[Tb(\mathbf{hpb})(OH)(MeO)]Na^+ \cdot 3MeOH$	597.1	597.0
$[Tb(\mathbf{hpb})_2(H_2O)]^+$	719.2	720.8
$[Tb(\mathbf{hpb})_2(H_2O)]Na^+ \cdot MeOH$	751.2	752.8
$[Tb_4(OH)_2(O)(\mathbf{hpb})_6]^{2+}$	1157.3	1157.4
$[Tb_4(OH)_2(O)(\mathbf{hpb})_6]^{2+} \cdot 6MeOH$	1253.3	1252.8
$[Er(\mathbf{hpb})(OH)(MeO)]Na^+ \cdot MeOH$	540.2	540.2
$[Er(\mathbf{hpb})(OH)(MeO)]Na^+ \cdot 2MeOH$	572.1	572.2
$[Er(\mathbf{hpb})(OH)(MeO)]Na^+ \cdot 3MeOH$	604.2	604.2
$[Er_2(O)(OH)(\mathbf{hpb})_3]Na^+$	1203.3	1203.4

Scheme 2. Fragmentation Pathway Observed for Clusters **1**−**4**

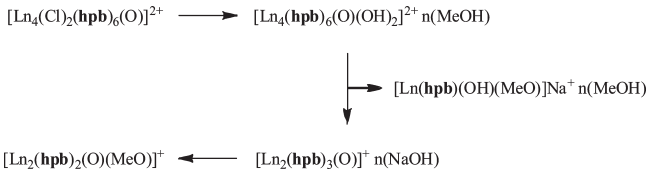

The chloride bridged dicationic species $[Ln_4(Cl)_2(O)(\mathbf{hpb})_6]^{2+}$ was observed only in the case of **1**. Rapid hydrolysis to an hydroxo bridged tetranuclear dication $[Ln_4(OH)_2(O)(\mathbf{hpb})_6]^{2+}$ was instead observed for **1**−**3**. Fragmentation of this species was found to produce one of two possible cationic species, a mononuclear cation, $[Ln(\mathbf{hpb})(OH)(MeO)]Na^+$, seen as dominant peaks corresponding to methanol solvates, and the dimeric species $[Ln_2(O)(\mathbf{hpb})_3]^+$ observed for both **1** and **4**. Displacement of a single ligand by methanol or water gave the final dimeric cation observed $[Nd_2(O)(\mathbf{hpb})_2(OR)]^+$ (R = H, Me). While there was no direct evidence of tetranuclear species for erbium cluster **4** by ESI-MS, comparison of the Raman spectrum with that of holmium cluster **2** (Figure 3) gives considerable evidence to support the presence of an identical core motif.

Varying the ligand to contain a *p*-methoxy phenyl group (**Hhmb**) resulted in marked changes to the composition of the cluster. Single crystals of compounds **5** and **7** were obtained by slow evaporation of toluene solutions of these compounds. X-ray crystallography determinations on compounds **5** and **7** showed that they exhibit the same cationic dimeric motif (Figure 4) with a varying number of solvent molecules located in the crystal lattice. Terbium cluster **7** is representative of series **5**−**9** as determined by mass spectrometry, infrared spectroscopy, and elemental analyses and is discussed in further detail below. Only the X-ray crystal structure of compound **7** will be discussed here, while the data for compound **5** are available as Supporting Information.

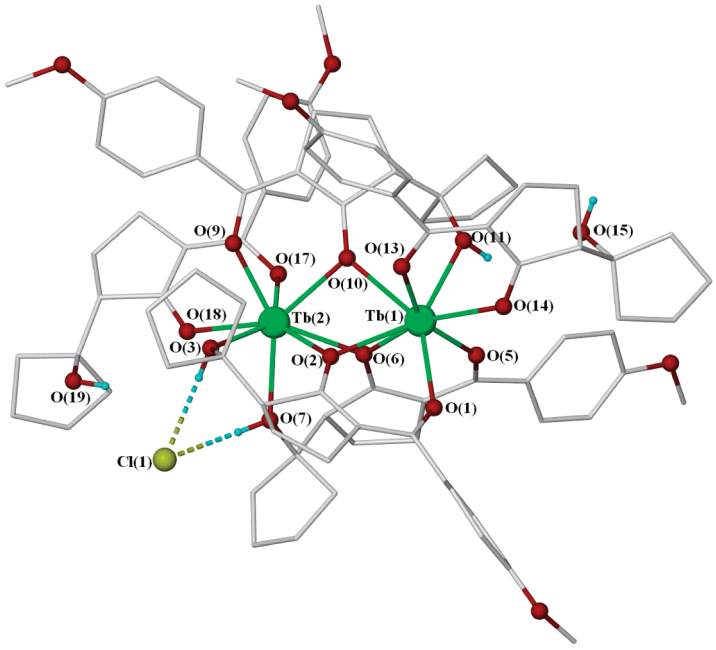

Figure 4. Molecular structure of **7**. Lattice solvent and hydrogen atoms (excluding hydroxy) have been omitted for clarity. The structure of compound **5** is similar.

Table 3. Selected Bond Lengths and Angles for **7**

Bond Lengths, Å			
Tb(1)−O(1)	2.311(5)	Tb(2)−O(2)	2.412(5)
Tb(1)−O(2)	2.456(5)	Tb(2)−O(3)	2.430(6)
Tb(1)−O(5)	2.337(5)	Tb(2)−O(6)	2.415(5)
Tb(1)−O(6)	2.397(5)	Tb(2)−O(7)	2.413(6)
Tb(1)−O(10)	2.424(5)	Tb(2)−O(9)	2.286(6)
Tb(1)−O(11)	2.417(5)	Tb(2)−O(10)	2.398(5)
Tb(1)−O(13)	2.291(6)	Tb(2)−O(17)	2.272(6)
Tb(1)−O(14)	2.313(5)	Tb(2)−O(18)	2.332(6)
Bond Angles, deg			
O(1)−Tb(1)−O(2)	71.84(18)	O(17)−Tb(2)−O(18)	74.4(2)
O(2)−Tb(2)−O(3)	73.86(18)	Tb(1)−O(2)−Tb(2)	99.1(2)
O(5)−Tb(1)−O(6)	70.43(19)	Tb(1)−O(6)−Tb(2)	100.7(2)
O(9)−Tb(2)−O(10)	73.29(19)	Tb(1)−O(10)−Tb(2)	100.4(2)
O(10)−Tb(1)−O(11)	72.85(18)		

The structure of **7** can be seen in Figure 4, and a selection of bond lengths and angles are given in Table 3. Unlike the cluster structure obtained using the **Hhpb** ligand, the addition of the MeO group in the para position in **Hhmb** has resulted in the formation of a dinuclear complex of composition $[\{Tb_2(\mathbf{hmb})_5\}Cl\cdot(toluene)_2]$. The two metal centers are μ_2-bridged by the central O atoms of three ligands with average Tb−O distances of 2.43 Å and near identical Tb−O−Tb angles of 99.1(2)°, 100.7(2)°, and 100.4(2)° for O(2, 6, and 10). These three ligands have overall binding modes of μ_2-η^2(O,O′)η^2(O′,OH), as was seen in **1**. The outer O atoms of the diketyl groups are the shorter, averaging 2.31 Å, with the Tb−O(hydroxy) bonds averaging 2.42 Å. The average diketyl 'bite' angles are 71.9°, which is not significantly different from the hydroxy contained bite angles, which average 72.5°. Tb(1) is bonded to two ligands in an η^2(O,O′) fashion and one via η^2(O′,OH) bonding. The reverse, however, is true for Tb(2), and the two hydroxy groups which are bound to the Tb(2) hydrogen-bond to the Cl anion with donor−acceptor distances of 3.021(6) Å and 3.058(7) Å. The remaining two ligands can be considered as capping, as they bond to only one metal each with an overall bonding mode of η^2(O,O′). These are more symmetrical interactions with outer Tb−O bonds of 2.291(6) Å and 2.272(6) Å and central Tb−O bonds of 2.313(5) Å and 2.332(16) Å. The respective bite angles are 73.3(2)° and 74.4(2)°. A single hydroxy group from a capping ligand hydrogen-bonds to a chloride associated with a neighboring cluster (donor−acceptor distance 3.213(7) Å), forming a pseudo polymer in the solid state (Figure 5).

In compounds **5**−**9**, the 5-hydroxy-1,3-diketonate **hmb** anion binds by two different coordination modes: (a) as a double chelator μ_2-η^2(O,O′)η^2(O′,OH) or (b) as a bidentate nonbridging ligand η^2(O,O′) (Figure 6). In compounds **1**−**4**, however, only coordination mode (a) is observed.

The infrared spectra for complexes **5**−**9** show intense bands at 1585 and 1553 cm^{-1}, indicative of the ν(C═O) and ν(C═C) vibrations. These bands are shifted to lower wavenumbers relative to the ligand where they appear as an unresolved broad band at 1598 cm^{-1}. Most of the observed bands mirror those seen for clusters **1**−**4**, with the exception of a well-defined *para*-substituted out of plane stretch observed at 840 cm^{-1}.[33,34]

The thermogravimetric plots obtained for dimeric species **5**−**9** dried *in vacuo* display dramatic losses in weight percentage between 100 and 300 °C. A thermal loss of lattice bound toluene molecules (onset temp: 50−110 °C) was found to overlap with the first decomposition loss of 18% (onset temp: 116 °C), hindering accurate determination of lattice bound solvents. A second weight loss of between 14 and 24% occurred at approximately 280 °C. Displacement of a bidentate ligand gives a weight loss of 16%, consistent with the first weight loss. It is postulated that the second process is thermal cleavage of the remaining ligands to yield volatile anisole. Elemental analyses performed on the dried crystalline products gave results consistent with the solid-state dimer

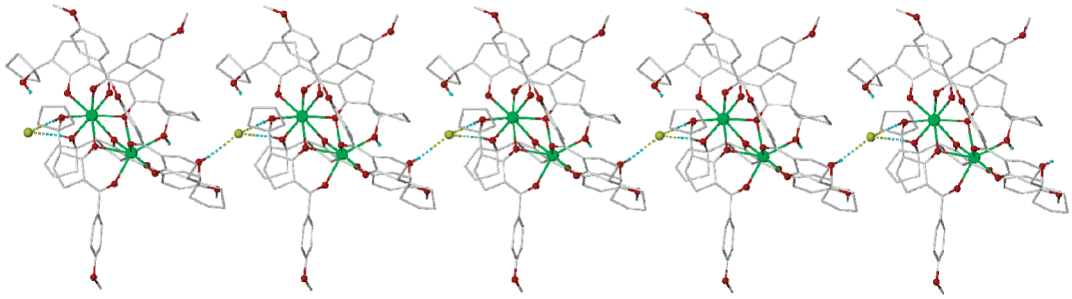

Figure 5. Extended structure of **7** showing hydrogen bonding interactions.

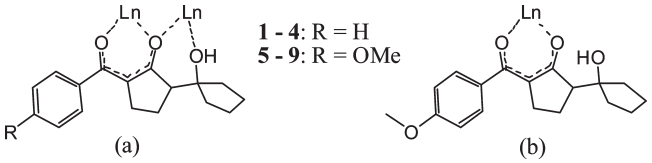

Figure 6. Coordination modes (a) μ_2-η^2(O,O′)η^2(O′,OH) and (b) η^2(O,O′) observed in lanthanoid species reported.

structures. The number of toluene molecules evident was in all cases lower than that predicted by TGA, suggesting that the lattice solvent is slowly lost *in vacuo*.

The clusters **5**−**9** were observed by ESI-MS as both cations and dications. Cationic species corresponding with fragmentation of the cluster were in most instances also observed. A less complex fragmentation pathway was observed than for clusters **1**−**4**, whereby the multiply ionized cluster cleaves to yield a combination of fragments including $[Ln(\mathbf{hmb})_2]^+$, $[Ln(\mathbf{hmb})_3]H^+$, and $[Ln(\mathbf{hmb})_4]2H^+$. A complete list of observed fragments is provided in the Supporting Information, as are the crystal data for **5**.

The $\chi_M T$ value of 25.9 cm^3 K mol^{-1} determined at 300 K for dimer **7** is typical of two uncoupled Tb^{III} ions, free of magnetic exchange interactions. Across the range of 300 to 100 K, the nature of χT was found to be largely temperature independent, which suggests a total population of all spin states and that magnetic interactions between the two Tb^{III} ions are very weak. Below 50 K, however, the χT value decreases rapidly down to 18.1 cm^3 K mol^{-1} at 5 K, which may be attributed to the depopulation of the Stark sublevels of the Tb^{III} ions. From this investigation, it has been concluded that the coupling between the Tb^{III} ions is very weak, and the observed decrease in χT at lower temperatures is predominantly due to thermal depopulation of the Stark sublevels originating from the Tb^{III} single ion, generated when the free ion states are split by field and spin−orbit coupling effects. Similar effects and conclusions have been observed in both tetranuclear and mononuclear Tb^{III} compounds reported in the literature.[36−38] An expanded discussion and plot of molar magnetic susceptibility and $\chi_M T$ vs T for **7** can be found as Supporting Information.

The postulated mechanism for the observed tetranuclear clusters **1**−**4** and dimeric species **5**−**9** entails formation of a dimeric species stabilized by three tridentated ligands (intermediate **A**; Figure 7). With the assumption that the coordination number of the lanthanoid centers remains constant throughout the synthesis, coordination of the three ligands to two $[LnCl_2(H_2O)_6]Cl$ units under basic conditions results in displacement of three chloride ions and 11 coordinated water molecules. The exchange of coordinated water molecules for the ligands (intermediate **A**) likely occurs due to favorable changes in entropy, as predicted by the chelate effect.[35] Two base mediated pathways continue from intermediate **A**: either fusion with a second equivalent of intermediate **A** mediated by deprotonation of the single coordinated water, yielding the cationic cluster motif **B** after liberation of one equivalent of water, or displacement of the remaining coordinated chlorides and water molecule by two equivalents of the ligand, resulting in the cationic dimer motif **C**. The choice of pathway likely depends on numerous factors such as identity of the ligand and differing solubilities of both intermediates and products. In either case, cationic products are generated due to the inability of the base to penetrate the sterically bulky cyclopentane rings capping each coordinated hydroxy group. As a result, the periphery of the cluster is stabilized by sterically demanding, monoanionic ligands which crowd the coordination sphere of the core, while minimizing counteraction of charge.

In addition to demonstrating control over the cationic nature of the products, the first example of synthesis of tetrameric motif **B** using an air- and moisture-stable methodology is detailed. Prior reports of analogous chloride bridged tetrameric species are typically air-sensitive[39−46] or partially hydrolyzed products of air-sensitive reaction mixtures.[47,48] We have established that hydrated lanthanoid chloride salts can be employed to synthesize such clusters, provided the number of intermediate coordinated water molecules can be limited and monoanionic charge on the ligands maintained.

(35) Schwarzenbach, G. *Helv. Chim. Acta* **1952**, *35*, 2344.
(36) Chen, X.-M.; Wu, Y.-L.; Tong, Y.-X.; Sun, Z.; Hendrickson, D. N.. *Polyhedron* **1997**, *16*, 4265.
(37) Bircher, R.; Abrahams, B. F.; Güdel, H. U.; Boskovic, C. *Polyhedron* **2007**, *26*, 3028.
(38) Caneschi, A.; Dei, A.; Gatteschi, D.; Poussereau, S.; Sorace, L. *Dalton Trans.* **2004**, 1048.
(39) Evans, W. J.; Sollberger, M. S.; Hanusa, T. P. *J. Am. Chem. Soc.* **1988**, *110*, 1841.
(40) Zhou, X.; Ma, H.; Wu, Z.; You, X.; Xu, Z.; Huang, X. *J. Organomet. Chem.* **1995**, *503*, 11.
(41) Wang, J.; Li, S.; Zheng, C.; Li, A.; Hosmane, N. S.; Maguire, J. A.; Roesky, H. W.; Cummins, C. C.; Kaim, W. *Organometallics* **2004**, *23*, 4621.
(42) Wang, J.; Li, S.; Zheng, C.; Hosmane, N. S.; Maguire, J. A.; Roesky, H. W.; Cummins, C. C.; Kaim, W. *Organometallics* **2003**, *22*, 4390.
(43) Zhong-Sheng, J.; Jing-Wen, G.; Ge-Cheng, W.; Jing-Yu, H.; Qi, S. *Chin. J. Struct. Chem.* **1990**, *9*, 140.
(44) Ji-Zhu, J.; Ge-Cheng, W.; Zhong-Sheng, J.; Wen-Qi, C. *Chin. J. Struct. Chem.* **1992**, *11*, 369.
(45) Jing-Wen, G.; Qi, S.; Jing-Yu, H.; Yong-Hua, L. *Chin. J. Struct. Chem.* **1990**, *9*, 184.
(46) Xiang-Gao, L.; Jing-Zhi, L.; Shong-Chen, J.; Yong-Hua, L.; Guo-Zhi, L. *Chin. J. Struct. Chem.* **1991**, *10*, 60.
(47) Pi, C.; Wan, L.; Gu, Y.; Zheng, W.; Weng, L.; Chen, Z.; Wu, L. *Inorg. Chem.* **2008**, *47*, 9739.
(48) Coles, M. P.; Hitchcock, P. B. *Inorg. Chim. Acta* **2004**, *357*, 4330.

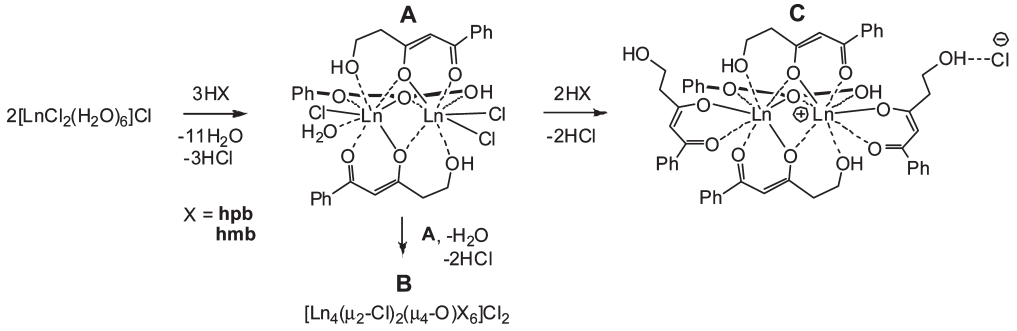

Figure 7. Postulated mechanism for the formation of tetrameric (**B**) and dimeric (**C**) motifs from a common precursor **A**. The omission of cyclopentane rings and replacement of the farthest ligand of intermediate **A** with a bold annotated line has been undertaken for clarity. Each step is base-mediated.

Conclusions

We have shown that 5-hydroxy-1,3-diketonate ligands stabilize cationic lanthanoid clusters. When treated with rare earth salts, (*R*/*S*,*Z*)-1′-hydroxy-3 (hydroxy(phenyl)methylene)-bi(cyclopentan)-2-one (**Hhpb**) and the closely related *p*-methoxyphenyl derivative (**Hhmb**) yielded tetranuclear and dinuclear clusters, respectively. These are identified as $[Ln_4(Cl_2)(O)(\mathbf{hpb})_6]Cl_2$ (Ln = Nd (**1**), Ho (**2**), Tb (**3**), and Er (**4**)) and $[Ln_2(\mathbf{hmb})_5]Cl$ (Ln = La (**5**), Nd (**6**), Tb (**7**), Dy (**8**), and Er (**9**)). The cluster motif was found to change dependent on the size and shape of the ligand; for example, the tetranuclear compound adopts a tetrahedral motif stabilized by coordination of the 5-hydroxyl group. Taken collectively, the clusters provide the first successful attempt at synthesizing and stabilizing cationic lanthanoid clusters through using specifically tailored diketonate ligands.

Experimental Section

Materials and Equipment. Chemicals were purchased from Sigma-Aldrich and were used as received. Solvents used were reagent grade and purified by usual methods. ^{1}H and ^{13}C NMR spectra were recorded on a Bruker AM 300 spectrometer and Varian Unity Nova 500 spectrometer. Chemical shifts were recorded on the δ scale and referenced against the solvent. Protons and carbons are labeled according to the crystallographic labeling in Figure 1. Solid-state IR spectra were recorded on a Bruker Equinox 55 Infrared Spectrometer fitted with a Specac Diamond ATR source. Raman spectroscopy was performed with either a Renishaw RM2000 spectrometer fitted with a 782 nm Renishaw diode laser or a Renishaw Invia spectrometer fitted with a 514 nm argon ion laser. TGA analyses was performed using a Setaram TG92 instrument with a heating rate of 10 K/min under nitrogen in a range from 50 to 650 °C. Melting points were measured on an SMP3 Stuart Scientific Melting Point Apparatus in an open capillary and were uncalibrated. Elemental analyses were performed by Campbell Microanalytical Laboratory, Department of Chemistry, University of Otago, Dunedin, New Zealand. Powder diffraction analyses were attempted on the crude microcrystalline samples (Ho, Tb, and Er), and the more prominent features predicted by LAZY Pulverix from the single crystal of the Nd species were observed, albeit with broadening of the diffractogram peaks. The samples subjected to powder diffraction were bulk crude samples and were not recrystallized in the same manner as the samples used for single crystal X-ray diffraction, and therefore some amorphous material is probably present, broadening the peaks.

Synthesis of Hhpb and Hhmb. To an anhydrous THF (5 mL) solution of cyclopentanone (0.33 g, 4.0 mmol) cooled to −78 °C was added LiHMDS (2.5 mL, 1.6 M in hexanes, 4.0 mmol). One equivalent of acid chloride (0.56 g, 4.0 mmol of benzoyl chloride for **Hhpb** or 0.68 g, 4.0 mmol of p-anisoyl chloride for **Hhmb**) was next added with rapid stirring. After one minute, two further equivalents of LiHMDS (5.0 mL, 8 mmol) were added in one portion followed by stirring for an additional minute. A second equivalent of cyclopentanone (0.33 g, 4.0 mmol) was added and the solution allowed to warm to room temperature. The reaction was quenched with water (~10 mL) and acidified to pH 5 with 1 M HCl. The solution was extracted with ethyl acetate (3× 50 mL) and the organic extracts dried ($MgSO_4$) and concentrated to dryness under reduced pressure. The crude product was then purified by column chromatography yielding the 5-hydroxy-1,3-diketone.

(*R*/*S*,*Z*)-1′-Hydroxy-3-(hydroxy(phenyl)methylene)bi(cyclopentan)-2-one (Hhpb). Orange crystals (0.61 g, 56% yield). Mp: 86.3−87.3 °C. ^{1}H NMR ($CDCl_3$): δ (ppm) 1.69 (m, 2H, H_{11}), 1.92 (dp, 4H, J = 8.0 Hz, H_{15} H_{16}), 2.26 (m, 2H, H_{10} H_{12B}), 2.47 (t, 2H, J = 8.0 Hz, H_{17}), 2.51 (m, 1H, H_{12A}), 2.78 (s, 1H, O*H*), 2.85 (t, J = 7.5 Hz, H_{14}), 7.43 (m, 3H, *m*-Ph*H* *p*-Ph*H*), 7.75 (d, 2H, J = 6.0 Hz, *o*-Ph*H*), 14.49 (s, 1H, O*H*). ^{13}C NMR ($CDCl_3$): δ (ppm) 23.85 (C_{16}); 24.01 (C_{15}); 24.84 (C_{12}); 26.34 (C_{11}); 36.20 (C_{14}); 56.02 (C_{17}); 82.94 (C_{10}); 110.02 (C_8); 128.20 (C_3 C_7); 128.38 (C_4 C_6); 131.22 (C_2); 134.23 (C_5); 169.14 (C_1); 211.59 (C_9). IR (KBr): 3566s, 3447m, 2961m, 2873m, 1639s, 1607s, 1588s, 1568s, 1491m, 1472w, 1448m, 1365s, 1331m, 1279m, 1184m, 1163m, 1141m, 1083m, 1029w, 1001w, 975w, 932w, 872m, 801m, 782m, 698s, 669w, 640w, 596w, 529w, 450w cm^{-1}. HRMS (ESI) calcd for $[M - H]^-$: 271.1334. Found: 271.1341.

(*R*/*S*,*Z*)-1′-Hydroxy-3-(hydroxy(4-methoxyphenyl)methylene)-bi(cyclopentan)-2-one (Hhmb). Yellow crystals (0.88 g, 73% yield). Mp: 61.8−62.8 °C. ^{1}H NMR ($CDCl_3$): δ 1.60 (m, 4H, H_{15} H_{16}); 1.85 (m, 4H, H_{14} H_{15}); 2.28 (m, 2H, H_{12}); 2.81 (m, 2H, H_{11}); 2.91 (dd, J_1 = 2.0, J_2 = 11.0 Hz, H_{10}); 3.51 (s, 1H, O*H*); 3.86 (s, 3H, CH_3); 6.96 (d, 2H, J = 9.0 Hz, Ph*H*); 7.77 (d, 2H, J = 9.0 Hz, Ph*H*); 14.64 (s, 1H, OH). ^{13}C NMR ($CDCl_3$): δ 24.14 (C_{16}); 24.27 (C_{15}); 25.00 (C_{12}); 26.81 (C_{11}); 36.30 (C_{14}); 38.90 (C_{17}); 55.65 (CH_3); 55.89 (C_{10}); 83.27 (C_{13}); 109.06 (C_8); 114.05 (C_4 C_6); 126.78 (C_2); 130.46 (C_3 C_7); 162.32 (C_5); 169.84 (C_1); 210.89 (C_9). IR (KBr): 3449m, 2954s, 2870m, 1733m, 1661m, 1598s, 1508s, 1455m, 1420w, 1374s, 1255s, 1172s, 1116s, 1061w, 1027m, 840m cm^{-1}. HRMS (ESI) calcd for $[M - H_2O]^+$: 285.1491. Found: 285.1484. HRMS (ESI) calcd for $[M + H]^+$: 303.1596. Found: 303.1594. HRMS (ESI) calcd for $[M + Na]^+$: 325.1416. Found: 325.1412.

General Procedure for Cluster Synthesis. To a round-bottomed flask equipped with a stirrer bead were added the relevant ligand and lanthanoid trichloride in a 2:1 molar ratio. The starting materials were dissolved in methanol, followed by a slow, dropwise addition of 4 equivalents of triethylamine. Reaction times unless otherwise stated were 24 h. After this time, the solvent was removed and the residue stirred in toluene (~2 mL) for 1 h. The solution was then filtered and left in an open vial to slowly evaporate.

[$Nd_4(Cl_2)(O)(hpb)_6]Cl_2$ (1). Pale yellow crystals. Yield: 24%. Mp: 210−215 °C (dec). Anal. calcd for $C_{102}H_{114}Cl_4Nd_4O_{19}\cdot 2H_2O$: C, 51.1; H, 5.0. Found: C, 51.1; H, 5.0. IR (ATR): 3057 m, 2946 m, 1592s, 1565s, 1494s, 1370s, 1313w, 1264s, 1073 m, 1026 m, 922w, 876w, 827m, 791m, 710s, 692s cm^{-1}. Raman: 1600, 1563, 1495, 1497, 1291, 1316, (br)1280, 1223, 1184, 1001, 879, 794, 568, 455, 128. MS (ESI) calcd for [Nd(**hpb**)(OH)(MeO)]$Na^+\cdot$MeOH: 516.1. Found: 516.2. MS (ESI) calcd for [Nd(**hpb**)(OH)(MeO)]$Na^+\cdot$3MeOH: 548.1. Found: 548.2. MS (ESI) calcd for [Nd(**hpb**)(OH)(MeO)]$Na^+\cdot$2MeOH: 580.2. Found: 580.2. MS (ESI) calcd for [Nd(**hpb**)$_2$(MeO)]Na^+: 738.2. Found: 738.1. MS (ESI) calcd for [Nd_2(O)(**hpb**)$_2$(MeO)]$^+$: 875.1. Found: 876.3. MS (ESI) calcd for [Nd_2(O)(**hpb**)$_3$]$^+$: 1115.5. Found: 1114.5. MS (ESI) calcd for [$Nd_4(Cl)_2$(O)(**hpb**)$_6$]$^{2+}$: 1143.7. Found: 1142.6. MS (ESI) calcd for [$Nd_4(OH)_2$(O)(**hpb**)$_6$]$^{2+}\cdot$2MeOH: 1157.7. Found: 1157.1. MS (ESI) calcd for [$Nd_4(OH)_2$(O)(**hpb**)$_6$]$^{2+}\cdot$6MeOH: 1222.3. Found: 1223.2.

[$Ho_4(Cl_2)(O)(hpb)_6]Cl_2$ (2). Orange powder. Yield: 65%. Mp: 215−220 °C (dec). Anal. calcd for $C_{102}H_{114}Cl_4Ho_4O_{19}\cdot$Tol: C, 51.4; H, 4.8. Found: C, 51.1; H, 4.3. IR (ATR): ν_{max} 2947m, 1596s, 1569s, 1495s, 1382s, 1314w, 1281s, 1074m, 1027m, 921w, 877w, 828m, 791m, 711s, 693s cm^{-1}. Raman: 1602, 1563, 1496, 1480, 1445, 1317, 1293, 1271, 1222, 1179, 1158, 1028, 1001, 880, 847, 794, 728, 719, 664, 618, 569, 516, 454, 404, 301, 270, 218, 130. MS (ESI) calcd for [Ho(**hpb**)(OH)(MeO)]$Na^+\cdot$MeOH: 539.1. Found: 539.2. MS (ESI) calcd for [Ho(**hpb**)(OH)(MeO)]$Na^+\cdot$2MeOH: 571.1. Found: 571.3. MS (ESI) calcd for [Ho(**hpb**)(OH)(MeO)]$Na^+\cdot$3MeOH: 603.2. Found: 603.2. MS (ESI) calcd for [$Ho_4(OH)_2$(O)(**hpb**)$_6$]$^{2+}\cdot$2MeOH: 1200.8. Found: 1201.2. MS (ESI) calcd for [$Ho_4(OH)_2$(O)(**hpb**)$_6$]$^{2+}\cdot$6MeOH: 1264.8. Found: 1265.1.

[$Tb_4(Cl_2)(O)(hpb)_6]Cl_2$ (3). Yellow powder. Yield: 58%. Mp: 215−225 °C (dec). Anal. calcd for $C_{102}H_{114}Cl_4Tb_4O_{19}\cdot H_2O$: C, 49.7; H, 4.7. Found: C, 49.7; H, 4.3. IR (ATR): ν_{max} 2947m, 1594s, 1569s, 1495s, 1378s, 1314w, 1281s, 1074m, 1026m, 922w, 877w, 828m, 791m, 711s, 693s cm^{-1}. Raman: 1601, 1497, 1445, 1316, 1273, 1273, 1162, 1146, 1027, 1002, 877, 834, 790, 618, 404, 270, 217. MS (ESI) calcd for [Tb(**hpb**)(OH)(MeO)]$Na^+\cdot$MeOH: 533.1. Found: 532.9. MS (ESI) calcd for [Tb(**hpb**)(OH)(MeO)]$Na^+\cdot$2MeOH: 565.1. Found: 564.9. MS (ESI) calcd for [Tb(**hpb**)(OH)(MeO)]$Na^+\cdot$3MeOH: 597.1. Found: 597.0. MS (ESI) calcd for [Tb(**hpb**)$_2$(H_2O)]$^+$: 719.2. Found: 720.8. MS (ESI) calcd for [Tb(**hpb**)$_2$(H_2O)]$Na^+\cdot$MeOH: 751.2. Found: 752.8. MS (ESI) calcd for [$Tb_4(OH)_2$(O)(**hpb**)$_6$]$^{2+}$: 1157.3. Found: 1157.4. MS (ESI) calcd for [$Tb_4(OH)_2$(O)(**hpb**)$_6$]$^{2+}\cdot$6MeOH: 1253.3. Found: 1252.8.

[$Er_4(Cl_2)(O)(hpb)_6]Cl_2$ (4). Orange powder. Yield: 60%. Mp: 220−225 °C (dec). Anal. calcd for $C_{102}H_{114}Cl_4Er_4O_{19}$: C, 50.3; H, 4.7. Found: C, 50.3; H, 4.2. IR (ATR): ν_{max} 2947m, 1594s, 1569s, 1495s, 1377s, 1315w, 1280s, 1074m, 1027m, 922w, 877w, 828m, 791m, 710s, 692s cm^{-1}. Raman: 1600, 1563, 1497, 1480, 1444, 1318, 1293, 1273, 1222, 1177, 1157, 1030, 1002, 876, 843, 795, 725, 720, 666, 618, 570, 512, 454, 405, 302, 267, 218, 131. MS (ESI) calcd for [Er(**hpb**)(OH)(MeO)]$Na^+\cdot$MeOH: 540.2. Found: 540.2. MS (ESI) calcd for [Er(**hpb**)(OH)(MeO)]$Na^+\cdot$2MeOH: 572.1. Found: 572.2. MS (ESI) calcd for [Er(**hpb**)(OH)(MeO)]$Na^+\cdot$3MeOH: 604.2. Found: 604.2. MS (ESI) calcd for [Er_2(O)(OH)(**hpb**)$_3$]Na^+: 1203.3. Found: 1203.4.

[La_2(hmb**)$_5$]Cl (5).** Yellow crystals. Yield 26%. Mp: 210−218 °C (dec). Anal. calcd for $C_{90}H_{110}ClLa_2O_{20}\cdot$Tol: C, 60.8; H, 6.2. Found: C, 60.1; H, 6.4. IR (ATR): ν_{max} 2944m, 1588s, 1554s, 1512w, 1434s, 1371s, 1307m, 1248s, 1168s, 1109w, 1029s, 841m cm^{-1}. MS (ESI) calcd for [La(**hmb**)$_2$]$^+$: 741.2. Found: 741.6. MS (ESI) calcd for [La(**hmb**)$_3$]H^+: 1043.3. Found: 1043.7. MS (ESI) calcd for [La(**hmb**)$_4$]$2H^+$: 1345.5. Found: 1347.0. MS (ESI) calcd for [La_2(**hmb**)$_5$]$^+$: 1783.5. Found: 1783.1.

[Nd_2(hmb**)$_5$]Cl (6).** Orange crystals. Yield 36%. Mp: 150−160 °C (dec). Anal. calcd for $C_{90}H_{110}ClNd_2O_{20}$: C, 58.9; H, 6.0. Found: C, 60.0; H, 6.2. IR (ATR): ν_{max} 2951m, 1585s, 1553s, 1433s, 1388s, 1305m, 1247s, 1167s, 1110w, 1023s, 975 m, 840m cm^{-1}. MS (ESI) calcd for [Nd(**hmb**)$_2$]$^+$: 744.2. Found: 744.5. MS (ESI) calcd for [Nd_2(**hmb**)$_5$Cl]$2Na^{2+}\cdot H_2O$: 945.2. Found: 945.4. MS (ESI) calcd for [Nd_2(**hmb**)$_5$Cl]$2Na^{2+}\cdot$(H_2O, EtOH): 968.3. Found: 969.4. MS (ESI) calcd for [Nd(**hmb**)$_3$]H^+: 1046.3. Found: 1046.7.

[Tb_2(hmb**)$_5$]Cl (7).** Yellow crystals. Yield 34%. Mp: 150−160 °C (dec). Anal. calcd for $C_{90}H_{110}ClTb_2O_{20}\cdot$2Tol: C, 61.0; H, 6.2. Found: C, 61.1; H, 6.2. IR (ATR): ν_{max} 2945m, 1587s, 1556s, 1513w, 1435s, 1381s, 1304m, 1247s, 1167s, 1107w, 1026s, 975m, 840m cm^{-1}. MS (ESI) calcd for [Tb(**hmb**)$_2$]$^+$: 761.2. Found: 761.6. MS (ESI) calcd for [Tb(**hmb**)$_3$]H^+: 1063.4. Found: 1063.6. MS (ESI) calcd for [Tb(**hmb**)$_4$]$2H^+$: 1365.5. Found: 1365.9. MS (ESI) calcd for [Tb_2(**hmb**)$_5$]$^+$: 1823.6. Found: 1823.3.

[Dy_2(hmb**)$_5$]Cl (8).** Yellow crystals. Yield: 17%. Mp: 215−225 °C (dec). Anal. calcd for $C_{90}H_{110}ClDy_2O_{20}$: C, 62.5; H, 5.9. Found: C, 62.7; H, 6.0. IR (ATR): ν_{max} 2945m, 1588s, 1559s, 1513w, 1433s, 1371s, 1306m, 1246s, 1166s, 1107w, 1026s, 987m, 838m, 764m, 716m, 666m, 621m cm^{-1}. MS (ESI) calcd for [Dy_2(**hmb**)$_5$Cl]$2Na^{2+}\cdot 3H_2O$: 983.3. Found: 983.5. MS (ESI) calcd for [Dy_2(**hmb**)$_5$Cl]$2Na^{2+}\cdot$($3H_2O$, EtOH): 1006.3. Found: 1006.1. MS (ESI) calcd for [Dy_2(**hmb**)$_5$Cl]$2Na^{2+}\cdot$($4H_2O$, EtOH): 1015.3. Found: 1016.4.

[Er_2(hmb**)$_5$]Cl (9).** Brown crystals. Yield 28%. Mp: 220−225 °C (dec). Anal. calcd for $C_{102}H_{114}Cl_4Er_4O_{19}$: C, 57.4; H, 5.9. Found: C, 57.8; H,5.7. IR (ATR): ν_{max} 2948m, 1589s, 1562s, 1513w, 1434s, 1378s, 1290m, 1246s, 1167s, 1108w, 1027s, 911w, 838m, 761m, 717m, 664w, 622m cm^{-1}. MS (ESI) calcd for [Er_2(**hmb**)$_5$]Na^{2+}: 931.3. Found: 930.1. MS (ESI) calcd for [Er_2(**hmb**)$_5$Cl]$2Na^{2+}\cdot$(H_2O, EtOH): 992.3. Found: 992.2. MS (ESI) calcd for [Er_2(**hmb**)$_5$Cl]$2Na^{2+}\cdot$(H_2O, 2EtOH): 1015.8. Found: 1016.1. MS (ESI) calcd for [Er_2(**hmb**)$_5$Cl]$2Na^{2+}\cdot$($2H_2O$, 2EtOH): 1024.8. Found: 1025.1. MS (ESI) calcd for [Er(**hmb**)$_3$]H^+: 1072.4. Found: 1072.1. MS (ESI) calcd for [Er(**hmb**)$_4$]$2H^+$: 1374.5. Found: 1374.3.

X-Ray Crystallography. Crystalline samples of **Hhpb**, **1**, and **7** were mounted on glass fibers in viscous hydrocarbon oil. Crystal data were collected using either an Enraf-Nonius Kappa CCD or a Bruker X8 APEX CCD instrument with monochromated Mo Kα radiation, λ = 0.71073 Å. All data were collected at 123 K, maintained using an open flow of nitrogen from an Oxford Cryostreams cryostat. Structural solution and refinement was carried out using SHELXL-97[49] utilizing the graphical interface X-Seed.[50] Data were corrected for absorption using the SADABS[51] or SORTAV[52] packages. Data collection and refinement parameters are given in Table 4. Disordered solvent within the lattice of **1** was initially modeled as Et_2O and sustained refinement well; however it did not account for all residual electron density and encroached to closely to the main residue. No other solvent molecules sustained refinement, and therefore the residual electron density was removed using PLATON Squeeze. The electron/cell count was given as 258 and the solvent accessible void as 2270 $Å^3$. During refinement of the structure of **7**, considerable disorder in all of the toluene solvent molecules meant that disordered components did not sustain anisotropic refinement, and even when refined isotropically the phenyl rings had to be restrained as ideal hexagons. Disorder in the methoxy groups of ligands 1 and 5 was also refined isotropically. Their thermal parameters were refined collectively, and the coordinates of C92 and C92A were fixed together. The phenyl rings C12 to C17 were constrained using the ISOR command as they appeared to have a very small component of disorder; however this could not sustain refinement. Large amounts of thermal movement in the flexible 5-membered

(49) Sheldrick, G. M. *Acta Crystallogr., Sect. A* **2008**, *A64*, 112.
(50) Barbour, L. J. *XSEED: A graphical interface for use with the SHELX97 program suite*; University of Missouri: Columbia, MO, 1999.
(51) Sheldrick, G. M. *SADABS*, version 2.03; University of Göttingen: Göttingen, Germany, 1997.
(52) Blessing, R. H. *J. Appl. Crystallogr.* **1997**, *30*, 421.

Table 4. Crystallographic Data for **Hhpb**, **1**, **5**, **7**

complex	**Hhpb**	**1**	**5**	**7**
empirical formula	$C_{17}H_{20}O_3$	$C_{108}H_{128}Nd_4N_2O_{21}Cl_4$	$C_{215}H_{250}Cl_2La_4O_{40}$	$C_{104}H_{121}Tb_2O_{20}Cl$
fw	272.33	2508.88	4100.70	2044.30
cryst syst	monoclinic	monoclinic	triclinic	monoclinic
space group	$P2_1/n$	$C2/c$	$P\bar{1}$	$P2_1/c$
a/Å	6.7644(4)	29.0161(4)	14.5792(2)	13.94790(10)
b/Å	10.5736(6)	26.7506(3)	17.1037(2)	26.9161(3)
c/Å	19.6341(15)	16.0948(2)	22.3594(3)	24.7997(2)
α/deg	90	90	109.0739(5)	90
β/deg	93.811(2)	108.0286(8)	98.7864(6)	100.5081(4)
γ/deg	90	90	107.3747(5)	90
V/Å	1401.22(16)	11879.4(3)	4831.39(11)	9154.24(14)
Z	4	4	2	4
D_c/g cm^{-1}	1.291	1.403	1.409	1.483
μ/mm^{-1}	0.087	1.871	0.970	1.634
F(000)	584	5064	2122	4208
θ range/deg	2.08 to 25.00	1.06 to 25.00	1.36 to 25.00	1.51 to 25.00
R_{int}	0.0970	0.0794	0.0638	0.1151
final R indices [$I > 2\sigma(I)$]	$R_1 = 0.0687$, $wR_2 = 0.1878$	$R_1 = 0.0700$, $wR_2 = 0.1713$	$R_1 = 0.0622$, $wR_2 = 0.1831$	$R_1 = 0.0787$, $wR_2 = 0.2179$
GOF	0.997	1.196	1.050	1.092

rings have also led to somewhat large thermal ellipsoids; however this is common with such ligands, and further constraints would not give a realistic model of the complex.

Crystallographic data (excluding structure factors) for the structures reported in this paper have been deposited with the Cambridge Crystallographic Data Centre as supplementary numbers 763516−763519. Copies of the data can be obtained free of charge on application to CCDC, 12 Union Road, Cambridge, CB2 1EZ, U.K. (fax: +44 (0) 1223 336033; e-mail: deposit@ccdc.cam.ac.uk).

Acknowledgment. We gratefully thank Dr. Boujemaa Moubaraki for assistance with the magnetism measurements and acknowledge financial support from the Australian Research Council and Monash University.

Supporting Information Available: Assignment of charged species observed for clusters **5**−**9**, crystallographic data for **5**, and magnetic measurements for **7**. This material is available free of charge via the Internet at http://pubs.acs.org.